Quaternary Research (2024), **118**, 62–74
doi:10.1017/qua.2023.11

Research Article

The distribution of fossil pollen and charcoal in stalagmites

Bianca Dickson[1]*, J.M. Kale Sniderman[1], Vera A. Korasidis[1] and Jon Woodhead[1]

[1]The School of Geography, Earth, and Atmospheric Sciences, University of Melbourne, Parkville, VIC, 3010, Australia

Abstract

Pollen preserved in caves provides a little-appreciated opportunity to study past vegetation and climate changes in regions where conventional wetland sediments are either unavailable, contain little organic matter, and/or are difficult to date accurately. Most palynology in caves has focused on clastic infill sediments, but pollen preserved in growing speleothems provides important new opportunities to develop vegetation and climatic records that can be dated accurately with radiometric methods. However, when pollen is present in speleothems, concentrations can vary by orders of magnitude, highlighting how little we know about the processes that transport pollen into caves and onto speleothem surfaces, and that determine the pollen's preservation probability. To explore these aspects of speleothem pollen taphonomy, we investigated the distribution of pollen and microscopic charcoal within several stalagmites from southwest Australia. We examined spatial patterns in pollen and charcoal preservation in order to distinguish whether observed gradients result from preservation or are products of systematic transport processes working along stalagmite surfaces. We find that pollen grains and charcoal fragments are located preferentially on the flanks of most stalagmites. This suggests that pollen grain and charcoal deposition on speleothems is influenced by transport and accumulation of detrital debris on growing surfaces. These insights will assist in future sampling campaigns focusing on speleothem pollen and charcoal contents.

Keywords: Pollen, Charcoal, Taphonomy, Speleothem, Southwest Western Australia

(Received 9 November 2022; accepted 10 February 2023)

INTRODUCTION

Pollen analysis is widely used to study past vegetation and climate change, and the taphonomic processes that govern deposition and preservation of pollen in lacustrine and other wetland basins have been well understood for many decades. However, in some regions, wetlands and lakes are scarce or preserve very little organic material, limiting their potential for generating paleoenvironmental histories. If limestone cave systems are present, however, it may be possible to reconstruct past vegetation using fossil pollen trapped in growing speleothems (McGarry and Caseldine, 2004; Matley et al., 2020). Indeed, speleothem pollen records have an advantage, in that radiocarbon dating of wetland sediments depends on those sediments containing appreciable organic matter content, whereas speleothems can be dated accurately with U-Th and U-Pb methods well beyond the limits of the radiocarbon technique (Meyer et al., 2009; Sniderman et al., 2016). These advantages come into their own in regions such as southwest Western Australia, where wetlands and lakes are rare, and/or seasonal desiccation has destroyed most organic matter that might otherwise be preserved within existing wetland sediments.

Despite speleothem palynology's emerging importance, little is known about the taphonomic processes that influence pollen deposition onto, incorporation into, and preservation within speleothems (Burney and Burney, 1993; de Porras et al., 2011; Sniderman et al., 2019). To better understand pollen deposition and preservation within speleothems, here we map the concentration of pollen across and along growth axes within several stalagmites collected in caves in southwest Western Australia.

Previous speleothem palynological studies revealed that pollen is present in only a subset of speleothems within individual caves (Sniderman et al., 2016, 2019). Furthermore, pollen may be unevenly distributed within speleothems, with concentrations varying within a single speleothem by up to two orders of magnitude (Festi et al., 2016; Leutscher et al., 2021). It is unknown whether pollen is systematically concentrated in certain horizons, and if any correlation with dust content or other trace elements exists that could be used as a first-order indicator of pollen prospectivity. Clearly, a better knowledge of typical distribution patterns of pollen in speleothems would guide more effective micro-sampling.

During the initial stages of stalagmite preparation for generating vegetation histories from caves in southwest Western Australia, visual observations suggested that the flanks of stalagmites were 'dirty,' (i.e., they appeared to have greater concentrations of organic and/or siliciclastic matter than the central growth axes of the stalagmites; Supp. Fig. S1). Here we examine if this observation translates into higher pollen concentrations along the side growth flanks of stalagmites as compared to central growth axis, and whether this effect can be explained simply by greater dilution of detrital components in the faster-growing

*Corresponding author email address: dicksonb@student.unimelb.edu.au

Cite this article: Dickson B, Sniderman JMK, Korasidis VA, Woodhead J (2024). The distribution of fossil pollen and charcoal in stalagmites. *Quaternary Research* **118**, 62–74. https://doi.org/10.1017/qua.2023.11

axial region of the stalagmites. Other factors that could influence cave environments, and therefore speleothem pollen sequences, include the shapes of cave chambers, air circulation, and the presence of wildlife and vegetation types (McGarry and Caseldine, 2004). These factors may introduce biases in the representation of certain plant taxa relative to their abundance in surrounding vegetation (biases that also may be characteristic of lacustrine fossil pollen assemblages).

The concentration of charcoal trapped within stalagmites is also examined in this study. Both charcoal and pollen grains may be transported by the same vectors—wind and water—however charcoal is more resistant to degradation compared to pollen grains (Bryant and Holloway, 1983; Ascough et al., 2010; Scott 2010) and, over late Quaternary timescales, is generally treated as being entirely resistant to oxidative losses. By comparing the distribution patterns of both charcoal and pollen, we aim to determine how and if transport and preservation variables influence the taphonomy of pollen in speleothems. In addition, to explore the relationship, if any, between pollen and charcoal content and other indicators of speleothem 'dirtiness,' we analyzed likely aeolian-derived trace element concentrations in one of the stalagmites, along transects.

STUDY SITES

Naturally broken (i.e., fallen) speleothems used in this investigation were collected from Drovers Cave (30.26°S, 115.09°E, geographic projection WGS84 datum) and Mammoth Cave (34.06° S, 115.03°E, geographic projection WGS84 datum) in southwest Western Australia (Fig. 1). Appropriate sampling permits/permissions were in place for both locations. Drovers Cave is located on the northern Swan Coastal Plain and Mammoth Cave in the Leeuwin-Naturaliste region, both developed within the Tamala Limestone (Woodhead et al., 2022). The Tamala Limestone (Playford et al., 1976) is a predominantly Pleistocene aeolian calcarenite that extends for >1000 km along the Western Australian coast.

METHODS

We investigated the spatial distribution of fossil pollen grains between and along isochronous growth layers of four stalagmites.

Sampling

The stalagmites from Drovers Cave (stalagmites 6J-2-13, 6J-2-18, and 6J-2-19) were cut using a diamond rock saw to expose the internal face of the speleothem. A thin, central-axis slab was subsequently cut from the middle of the speleothem. On the surface of this central-axis slab, each stalagmite was divided into three columns (the left side flank, central growth axis, and right side flank). Each slab was serially sectioned, labelled, photographed, and measured (Fig. 2). Using a bandsaw, each middle slab also was cut into contiguous, stratigraphically isochronous subsamples. The subsamples were taken from the left side flank, central growth axis, and right side flank of each isochronous growth horizon and then measured and weighed. For the Mammoth Cave stalagmite (stalagmite MC1), only the left top portion of the stalagmite was available because portions of this stalagmite had been consumed in previous studies. The stalagmite was subsampled using the same process as above, but this stalagmite was divided into three different axes—the central growth axis and two left flanks of differing growth-layer steepness, relative to the central growth axis (Fig. 2). Because the stalagmites were collected in a broken state in their respective cave chambers, the 'left' and 'right' flank labels are arbitrary in this study and are used only to differentiate between the different sides of each stalagmite. The subsamples of both the Drovers Cave and Mammoth Cave stalagmites were analyzed for fossil pollen and charcoal concentration.

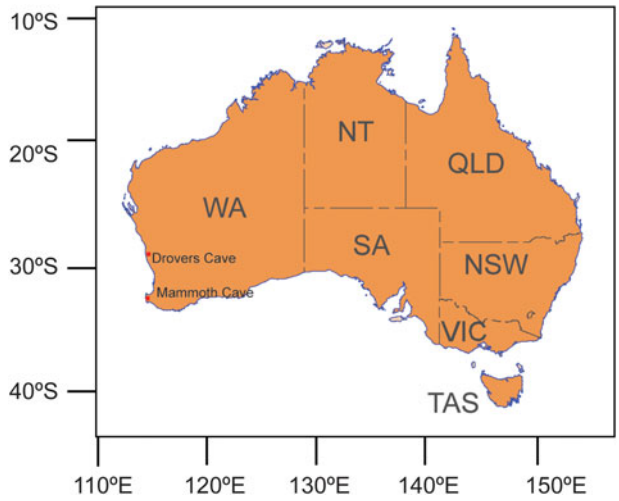

Figure 1. Location of the studied caves in Western Australia, Australia.

Palynological preparation

Palynological (pollen and charcoal) subsamples were processed using techniques adapted from Sniderman et al. (2016) that were designed to minimize contamination by modern pollen and maximize fossil pollen grain recovery from the speleothem. Following sawing, all subsequent processing procedures were conducted in a HEPA-filtered clean air fume hood within an Australian standard Class 350 (equivalent to ISO Class 7) clean room. Each subsample was washed in distilled water, then etched with 10% hydrochloric acid (HCl) for 10 minutes to remove any potential modern surface contamination and rinsed in distilled water. One exotic *Lycopodium* spore tablet (batch number 3862, reported to contain ca. 9666 ± 212 spores, Lund University) was added to each sample to allow for later calculation of pollen concentrations. Concentrated (10 M) HCl was added to the subsamples to dissolve them, the residues centrifuged, and the supernatants decanted and rinsed with distilled water. Concentrated hydrofluoric acid (HF) subsequently was added, left overnight, centrifuged, and decanted; 10% HCl subsequently was added to the subsamples, centrifuged, and decanted. Two drops of safranin stain were added to increase pollen grain visibility in the subsample. The subsamples were also dehydrated using ethanol and suspended in glycerol before mounting on glass slides.

Pollen analysis

Where possible, at least 100 pollen grains were counted for each subsample using a Zeiss Axio Lab A1 microscope with the aid of PolyCounter version 3.1.6 (Nakagawa, 2013). Pollen identification was made by comparisons with reference collections housed in the School of Geography, Earth and Atmospheric Sciences at the University of Melbourne, and with published pollen databases

https://doi.org/10.1017/qua.2023.11 Published online by Cambridge University Press

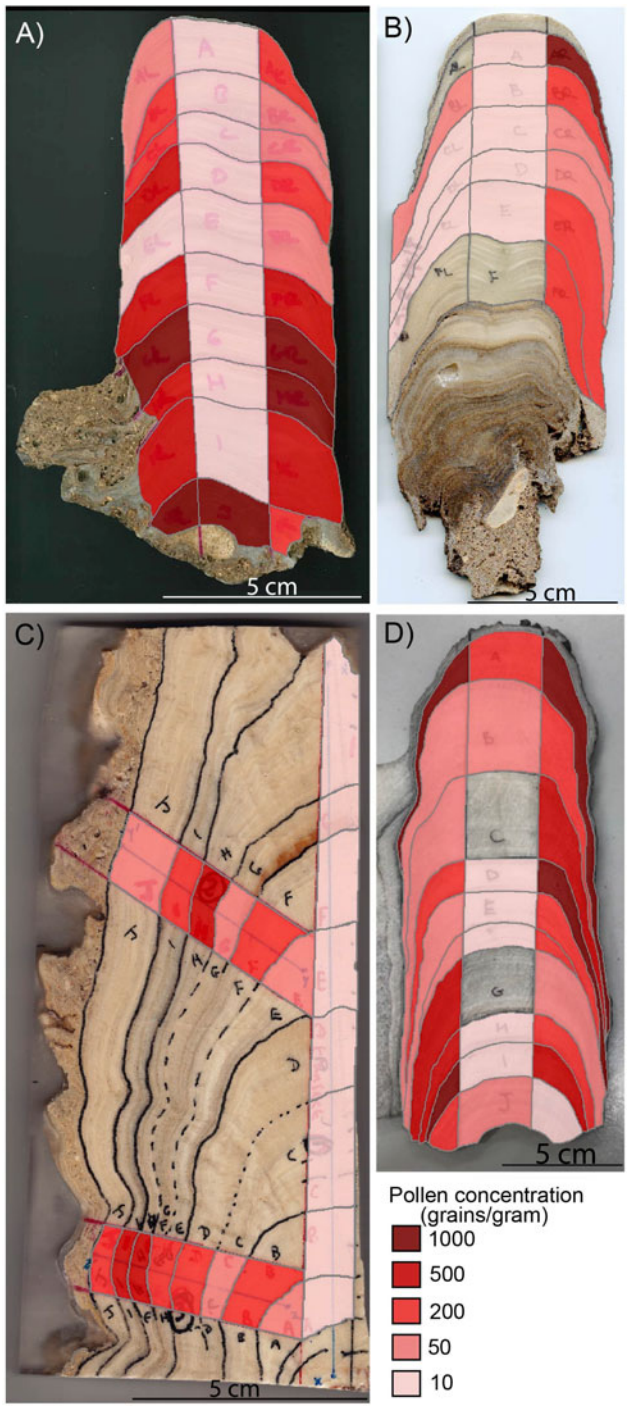

Figure 2. Heat map of pollen concentrations. The red-shaded areas indicate the center axis and side flank sections on the stalagmites that were analyzed in this study. (**A**) MC1, (**B**) 6J-2-13, (**C**) 6J-2-18, (**D**) 6J-2-19. Note, the two samples in 6J-2-19 that could not be processed are represented by the uncolored sections of the center axis of the stalagmite (C and G).

including the Australasian Pollen and Spore Atlas (APSA Members, 2007).

Charcoal analysis

Where possible, charcoal grains were counted on the same slides used for pollen analysis. Charcoal fragments were tallied until 100 *Lycopodium* spores were counted. This was also achieved using the same microscope and software described in the pollen analysis above.

Laser ablation inductively coupled plasma mass spectroscopy (LA-ICP-MS)

LA-ICP-MS was undertaken at the University of Melbourne following methods outlined in Woodhead et al. (2007) and performed using an Agilent 7700 inductively coupled plasma mass spectrometer. Trace element analysis was completed on the three axes of MC1 and 6J-2-13 (Supp. Fig. S1) to determine if there was any relationship between the trace element distribution along the flanks and center axis of the stalagmite and the corresponding pollen distributions. The following isotopes were measured, which include commonly used speleothem climate proxies and elements that might be considered indicators of aeolian dust fluxes: ^{43}Ca, ^{25}Mg, ^{27}Al, ^{29}Si, ^{88}Sr, ^{89}Y, ^{90}Zr, ^{138}Ba, ^{139}La, ^{232}Th, and ^{238}U.

Statistical analysis

Stratigraphic dips of growth horizons

To determine whether pollen and charcoal concentrations varied between growth axes and flanks, we investigated the relationship between pollen/charcoal concentrations and the average stratigraphic dip of each subsample, which we expected would serve as a proxy for the subsample's position along the growth surface of its stalagmite. That is, we expected that samples straddling the central growth axis have nearly horizontal dip, while samples on the flanks have steeper dip, and this difference conceivably may contribute to pollen/charcoal retention or loss. Using a line drawing rendered from the images of the stalagmites (Supp. Fig. S2), the average dip of each subsample was calculated by dividing upper or and lower curving subsample boundaries into a series of straight lines. We measured the dip of the constituent straight lines that define the growth layer, weighting them by their length (Supp. Fig. S2).

Normalizing data

To compare pollen and charcoal concentrations in each subsample with the stalagmite average, and with its horizon average, the concentration data (see Supp. Figs. S3, S4) were normalized, by dividing each subsample's pollen and charcoal concentrations by the average respective concentration of all the subsamples within that stalagmite. This was undertaken to remove the effect of differences in absolute pollen and charcoal concentrations between the stalagmites. This avoids the risk of some stalagmite results 'out-weighing' the results from the others and facilitates easier comparisons among the four stalagmites. For flank:central-axis comparison, the charcoal and pollen concentrations were normalized separately across each respective growth horizon to remove bias introduced by variation from horizon to horizon and to facilitate easier comparison of the axis of each stalagmite.

Ratio comparison of charcoal fragments and pollen grains

We also assessed whether the difference in charcoal and pollen concentrations along the central axis and side flanks potentially could be attributed to differing preservation conditions present in the stalagmite. To test this, the ratios between the pollen concentrations of central-axis subsamples and their corresponding isochronous flank subsamples were compared with the ratios

https://doi.org/10.1017/qua.2023.11 Published online by Cambridge University Press

for charcoal. The flank:central-axis ratios for charcoal concentration act as the baseline that, theoretically, can be attributed entirely to transfer of particles from the central axis to the flanks. If the flank:central-axis ratios for pollen concentration are indistinguishable from those for charcoal, this implies that pollen acts like a charcoal particle. Alternatively, if the ratios for pollen are larger than for charcoal, this implies there is a relative loss of pollen at the central axis, or a relative gain of pollen at the flanks, compared to charcoal. Growth layer subsamples were only included in this analysis if data of both flanks and the central growth axis were available. In the case of MC1, the far left flank and central axis were included in this analysis.

We also investigated whether the varying pollen concentrations along isochronous horizons might result from the changing subsample volumes because horizons are typically thinner, when moving from the center axis to the side flanks. We assessed this by investigating whether a relationship existed between the ratio of surface area of an isochronous flank and center subsample, and the ratio of pollen concentrations. The surface areas of the stalagmite subsamples were measured, and each area measurement was then compared to its corresponding pollen grain and charcoal flank:central-axis ratio.

RESULTS

Pollen and charcoal concentrations

Figures 2 and 3 are visual representations of the variations in the pollen and charcoal concentration along and between growth layers of the four stalagmites. Values for each subsample are included in Table 1.

Stalagmite MC1

The flanks and central axis studied in the MC1 stalagmite differ from those in the other three stalagmites in this study in that the MC1 stalagmite was already bisected along the center axis because the other half of the stalagmite was no longer available for analysis. In lieu of a symmetrical left side flank, central growth axis, and right side flank to study, two transects at different positions relative to the center axis were selected. These are herein referred to as the 'left' and 'far left' flanks. The central growth axis has the lowest concentrations of pollen and charcoal of the three axes, with average pollen concentration in the center axis of 22 pollen grains per gram (pollen/g), compared to the average flank pollen concentration of 352 pollen/g. A similar distribution pattern is also seen in the charcoal concentration results. The central axis has an average concentration of 47 charcoal fragments per gram (charcoal/g), compared to the average flank concentration of 411 charcoal/g.

Stalagmite 6J-2-13

Overall pollen concentrations are greater on both flanks of the stalagmite in comparison to the central axis. The older subsamples from the flanks of the stalagmite, layers F–J (Supp. Fig. S1), have a greater concentration of pollen than the upper portion of the subsamples. A clear difference is observed, with an average pollen concentration in the center axis of 269 pollen/g, compared to the average flank pollen concentration of 731 pollen/g. A similar distribution pattern is also seen in the charcoal concentration results, with an average of 12 charcoal/g along the central axis compared with the average flank concentration of 58 charcoal/g.

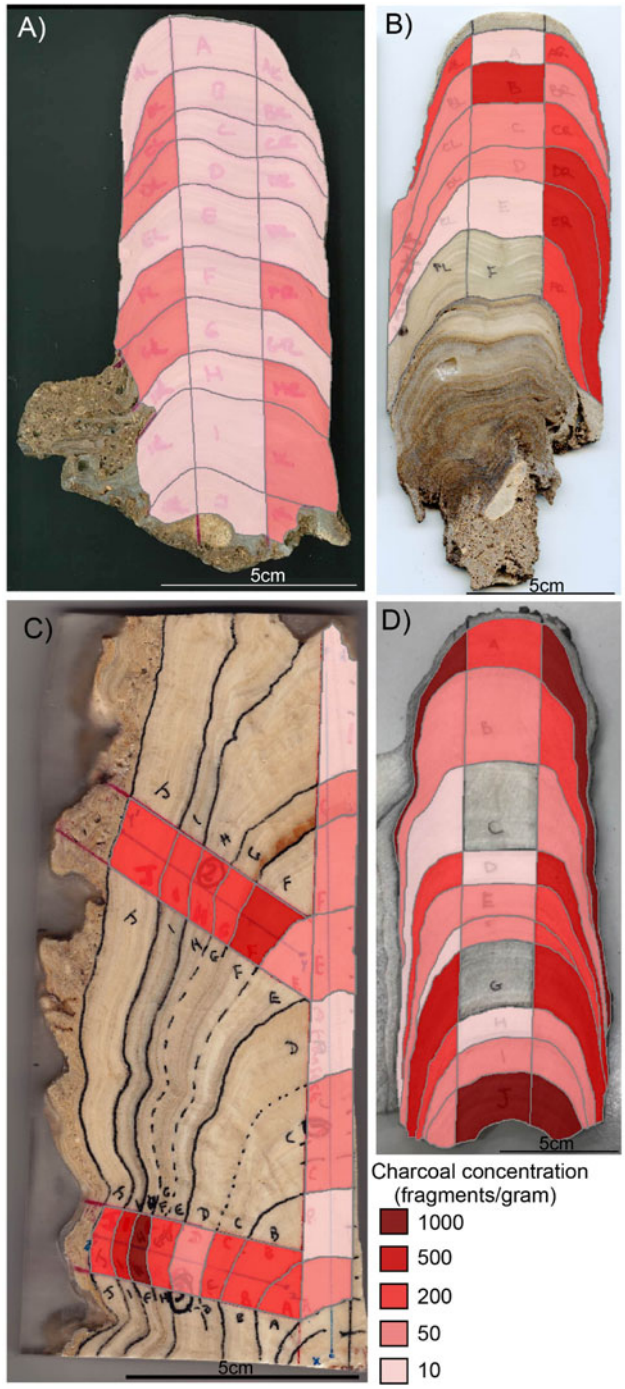

Figure 3. Heat map of charcoal concentrations. The red-shaded areas indicate the center axis and side flank sections on the stalagmite that were analyzed in this study. (**A**) MC1, (**B**) 6J-2-13, (**C**) 6J-2-18, (**D**) 6J-2-19. Note, the two samples in 6J-2-19 that could not be processed are represented by the uncolored sections of the center axis of the stalagmite (C and G).

Stalagmite 6J-2-18

The right flank of this stalagmite has the greatest concentration of pollen grains overall, with subsample AR containing the most pollen grains. Three subsamples AL, F, and FL, were not included because the subsample AL had extremely low pollen counts, and subsamples F and FL were not suitable for processing procedures. The lower portion of the stalagmite was

https://doi.org/10.1017/qua.2023.11 Published online by Cambridge University Press

Table 1. Charcoal and pollen concentration results.

	Pollen concentrations (grains/gram)				Charcoal concentration (grains/gram)			
Growth Horizon	Far left Side Flank	Left Side Flank	Central Growth Axis	Right Side Flank	Far left Side Flank	Left Side Flank	Central Growth Axis	Right Side Flank
MC1								
A	168		9		223		107	
B	249		32		458		25	
C	157		32		232		53	
D	394		8		155		24	
EFG	401	210	39		439	325	53	
H	870	537	10		1426	420	19	
I	561	235			528	204		
J	266	181			262	267		
6J-2-13								
A		146	22	228		11	25	46
B		293	14	162		93	3	21
C		390	25	141		126	18	14
D		604	23	414		119	7	20
E		31	8	61		25	11	9
F		829	18	898		51	13	83
G		1452	17	2109		65	5	39
H		783	27	1229		28	0	127
I		910	10	683		34	5	65
J		2807	2525	458		32	32	52
6J-2-18								
A			14	1070		207	21	427
B		168	2	207		133	534	200
C		30	7	125		169	54	316
D		11	9	88		70	92	934
E		3	4	240		8	36	658
F				389				376
6J-2-19								
A		1890	467	1484		1222	335	1564
B		147	118	312		157	179	250

C	99			570		38			191			
D	388		32	1128		208		42	954			
E	76		31	451		64		66	411			
F	136		10	303				62	354			
G	643			107		588			833			
H	606		40	220		419		49	68			
I	3086		40	510		155		184	183			
J	205		78	48		113		1074	1282			

not included in this analysis because the flanks and central axis could not be clearly defined. The central axis contained the lowest pollen concentration of 7 pollen/g, compared to the left flank average of 52 pollen/g and the right flank average of 353 pollen/g. There was a greater average charcoal concentration in the central axis (147 charcoal/ g) than the left flank charcoal concentration (117 charcoal/g). The right flank had an average of 485 charcoal/g.

Stalagmite 6J-2-19

Overall pollen concentrations are higher on the flanks of the stalagmite than on the central growth axis. The highest pollen concentrations are observed on the left side flank of the stalagmite. The lowest concentration throughout the stalagmite is the central growth axis with an average of 102 pollen/g, compared to the average flank pollen concentrations of 728 pollen/g on the left flank and 513 pollen/g on the right flank. Charcoal concentrations were higher on the flanks of the stalagmite than on the central axis. However, the right flank had the greatest charcoal concentration. The central axis had an average charcoal concentration of 248 charcoal/g compared to the average charcoal concentration of the right flank, which was 609 charcoal/g, and the left flank average concentration of 329 charcoal/g.

Patterns of pollen and charcoal in stalagmites

The average pollen concentration of each subsample was normalized to the concentration of each respective stalagmite to allow comparisons among stalagmites free of their differences in absolute pollen concentrations (Fig. 4). In general, higher concentrations of pollen grains occur on the flanks and lower concentrations occur on the central growth axis. This broad trend is reinforced when considering the average of both side flanks as opposed to presenting them separately. Each of the 95% confidence intervals of the side flanks overlap (Fig. 4), indicating that there is no discernible difference between the normalized pollen concentrations of the side flanks. However, the confidence intervals of the central growth axis do not overlap with any of the confidence intervals of the side flanks, indicating that the pollen concentrations along the central growth axis are lower than those of the side flanks.

The average charcoal concentration of each subsample was normalized to the concentration of each respective stalagmite to facilitate comparisons among stalagmites independent of their absolute charcoal concentrations (Fig. 5). In general, higher charcoal concentrations occur on the side flanks compared to the lower concentrations on the central growth axis (Fig. 5). The distribution of charcoal in 6J-2-18 has a slightly different pattern, with the charcoal concentration of the left side flank lower than in the central growth axis, however the concentration of the right side flank is much higher, and when comparing the normalized concentrations of both flanks to the concentration of the central axis (Fig. 5), there is still on average a higher charcoal concentration on the flanks of all the stalagmites in this study. Notably, all the 95% confidence intervals of the side flank charcoal concentrations of each stalagmite overlap. This indicates that there is no discernible difference between the normalized charcoal concentrations of the flanks on average (Fig. 5). However, the confidence intervals of the central growth axis do not overlap with any of the confidence intervals of the side flanks, indicating that the charcoal concentrations along the central growth axis are lower than those of the flanks.

https://doi.org/10.1017/qua.2023.11 Published online by Cambridge University Press

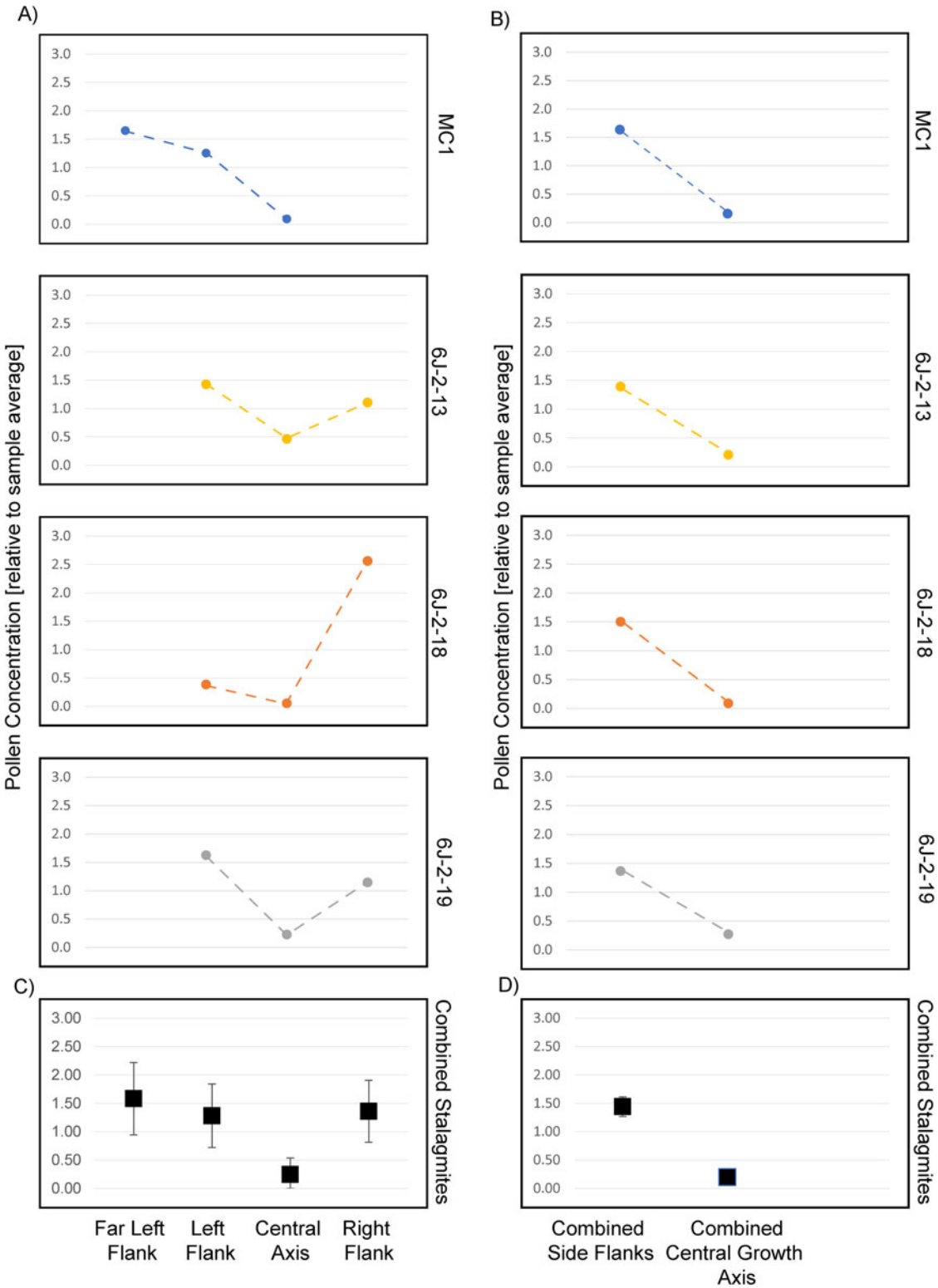

Figure 4. Normalized pollen concentrations of all the stalagmites in this study. (**A**) Average pollen concentration of each stalagmite normalized against each respective stalagmite; (**B**) comparison of normalized pollen concentrations of the side flanks combined and central growth axis of each stalagmite; (**C**) comparison of the average normalized pollen concentrations of each stalagmite with 95% confidence interval envelopes; and (**D**) comparison of the normalized pollen concentration of the side flanks combined and central growth axis of each stalagmite with 95% confidence envelopes. Any growth layers of the stalagmites that did not contain at least one flank and the center growth axis were excluded to avoid introducing a bias into the averages due to some missing data points.

https://doi.org/10.1017/qua.2023.11 Published online by Cambridge University Press

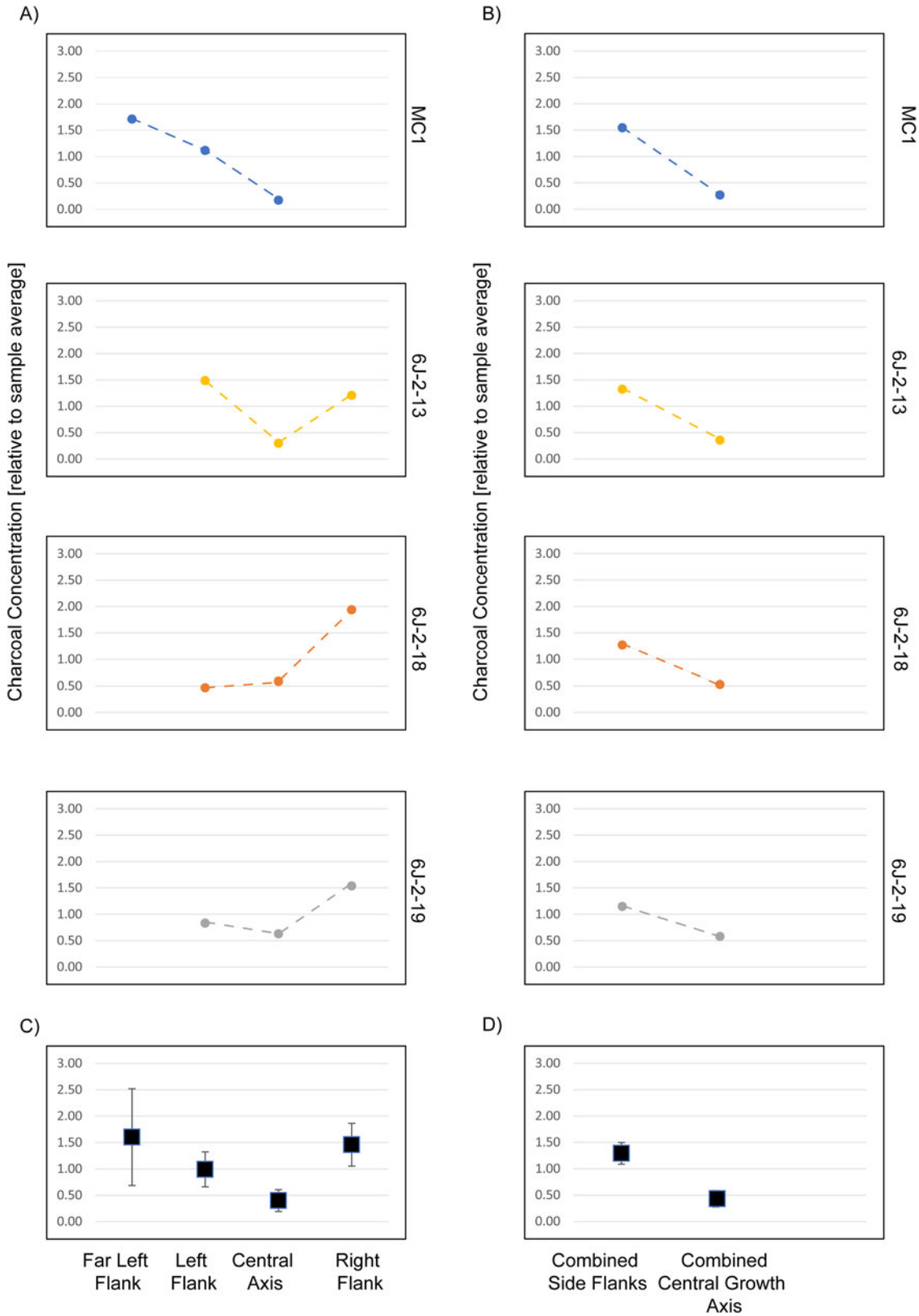

Figure 5. Normalized charcoal concentrations of all the stalagmites in this study. (**A**) Average charcoal concentration of each stalagmite normalized against each respective stalagmite; (**B**) comparison of normalized charcoal concentrations of the side flanks combined and central growth axis of each stalagmite; (**C**) comparison of the average charcoal concentrations of each stalagmite with 95% confidence interval envelopes, and (**D**) comparison of the normalized charcoal concentration of the side flanks combined and central growth axis of each stalagmite with 95% confidence envelopes. Any growth layers of the stalagmites that did not contain at least one flank and the center growth axis were excluded to avoid introducing a bias into the averages due to some missing data points.

https://doi.org/10.1017/qua.2023.11 Published online by Cambridge University Press

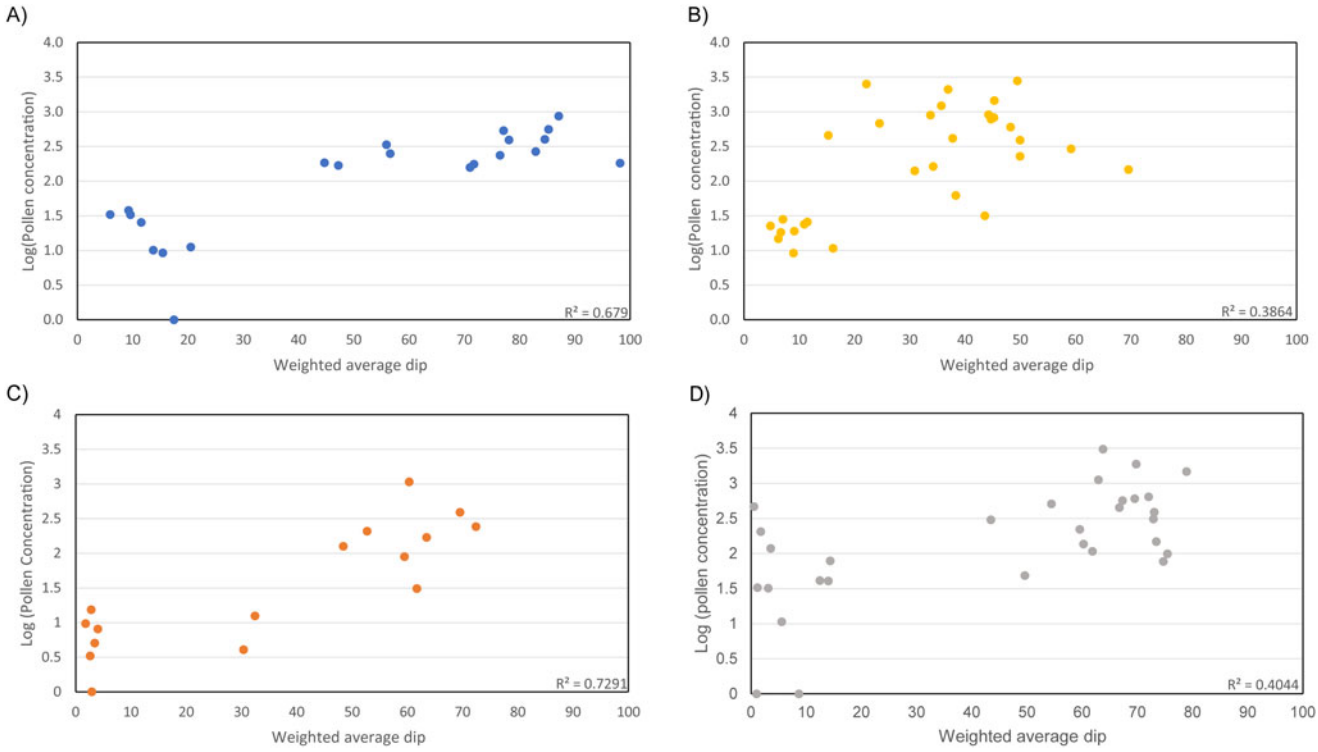

Figure 6. The stratigraphic dips of each sample compared to the log of pollen concentrations. (**A**) MC1, (**B**) 6J-2-13, (**C**) 6J-2-18, (**D**) 6J-2-19. Included in these plots are the R^2 values of ordinary least squares regression for each stalagmite.

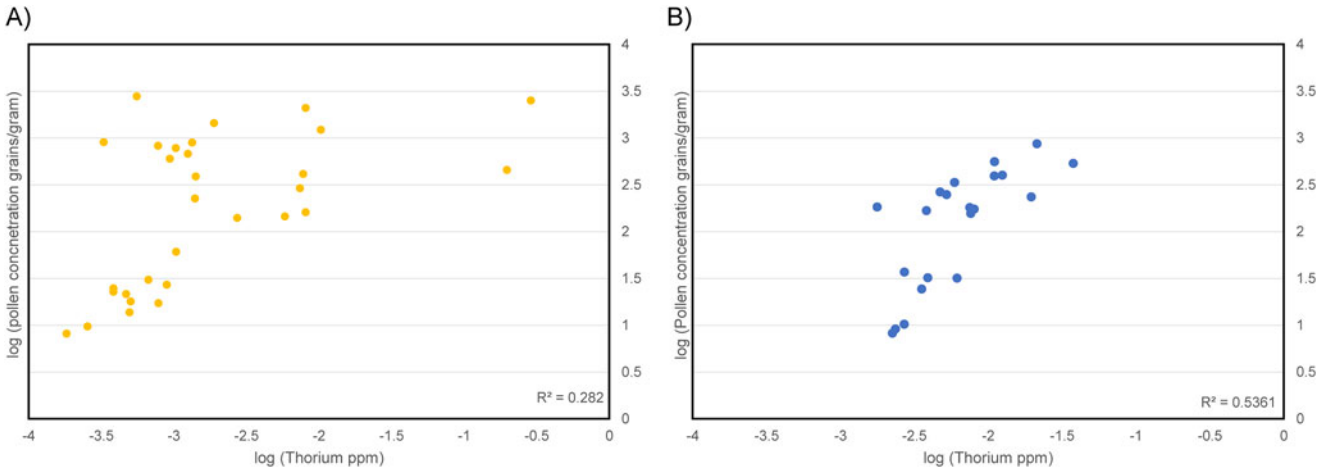

Figure 7. A comparison of Thorium and pollen concentrations on stalagmites. (**A**) 6J-2-13, (**B**) MC1.

Stratigraphic weighted average dip of growth horizons

In general, an increase in the stratigraphic dip of a sample is associated with an increase in the pollen concentration of the subsample (Fig. 6). This is consistent with the 'left, center, right' results included earlier.

Laser ablation analysis

We do see a relationship between the concentration of thorium and pollen concentration in the stalagmites MC1 and 6J-2-13 (Fig. 7). For MC1 and for 6J-2-13, the relationship is positive with an R^2 of 0.54 and 0.23, respectively. Thorium is highly insoluble in speleothem formation waters and high concentrations observed in speleothems are therefore a clear indication of the incorporation of aeolian or flood-derived dust components. These data suggest that dust content, as measured here with ^{232}Th, also may provide a useful indicator of pollen prospectivity.

Pollen concentration and area dilution ratio comparisons

The ratios of the pollen concentrations between isochronous flanks and center layers are larger than the corresponding charcoal concentration ratios (Table 2). Moreover, there is no clear relationship between the ratio of pollen concentration (flank:center) and the area ratio of the samples (flank:center) (Fig. 8). This

https://doi.org/10.1017/qua.2023.11 Published online by Cambridge University Press

Table 2. Ratio analysis of all stalagmites in this study. (**A**) Ratio of pollen grains (flank:center) compared to the ratio of charcoal fragments (flank:center), (**B**) ratio of pollen grains (flank:center) compared to the ratio of the area of samples (flank:center), and (**C**) ratio of charcoal fragments (flank:center) compared to the ratio of the area of samples (flank:center).

	A		B		C	
	Ratio of pollen flank:center	Ratio of charcoal flank:center	Ratio of pollen flank:center	Ratio of area flank:center	Ratio of charcoal flank:center	Ratio of area flank:center
MC1						
A	18.45	2.07	18.45	0.58	2.07	0.58
B	7.74	18.66	7.74	1.30	18.66	1.30
C	4.91	4.41	4.91	0.34	4.41	0.34
D	47.77	6.34	47.77	0.67	6.34	0.67
EFG	10.23	8.22	10.23	0.53	8.22	0.53
H	84.78	73.18	84.78	0.28	73.18	0.28
I						
J						
6J-2-13						
A	8.63	1.15	8.63	0.61	1.15	0.61
B	16.47	20.61	16.47	0.55	20.61	0.55
C	10.67	3.93	10.67	0.58	3.93	0.58
D	22.27	10.08	22.27	0.89	10.08	0.89
E	5.62	1.51	5.62	0.79	1.51	0.79
F	47.86	5.25	47.86	0.83	5.25	0.83
G	102.90	10.49	102.90	0.87	10.49	0.87
H			36.95	0.73		
I	81.45	10.14	81.45	0.87	10.14	0.87
J	0.65	1.33	0.65	0.46	1.33	0.46
6J-2-18						
A						
B	81.02	0.31	81.02	0.76	0.31	0.76
C	10.91	4.49	10.91	0.82	4.49	0.82
D	5.75	5.48	5.75	1.02	5.48	1.02
E	29.85	9.25	29.85	0.94	9.25	0.94
F						
6J-2-19						
A	3.61	4.15	3.61	0.76	4.15	0.76
B	1.95	1.14	1.95	0.60	1.14	0.60
C						
D	23.82	13.80	23.82	1.02	13.80	1.02
E	8.44	3.60	8.44	1.04	3.60	1.04
F			22.59	0.38		
G						
H	10.21	4.99	10.21	0.79	4.99	0.79
I	45.17	0.92	45.17	0.55	0.92	0.55
J	1.62	0.65	1.62	0.45	0.65	0.45
Average	**26.64**	**8.70**	**26.87**	**0.71**	**8.70**	**0.73**

https://doi.org/10.1017/qua.2023.11 Published online by Cambridge University Press

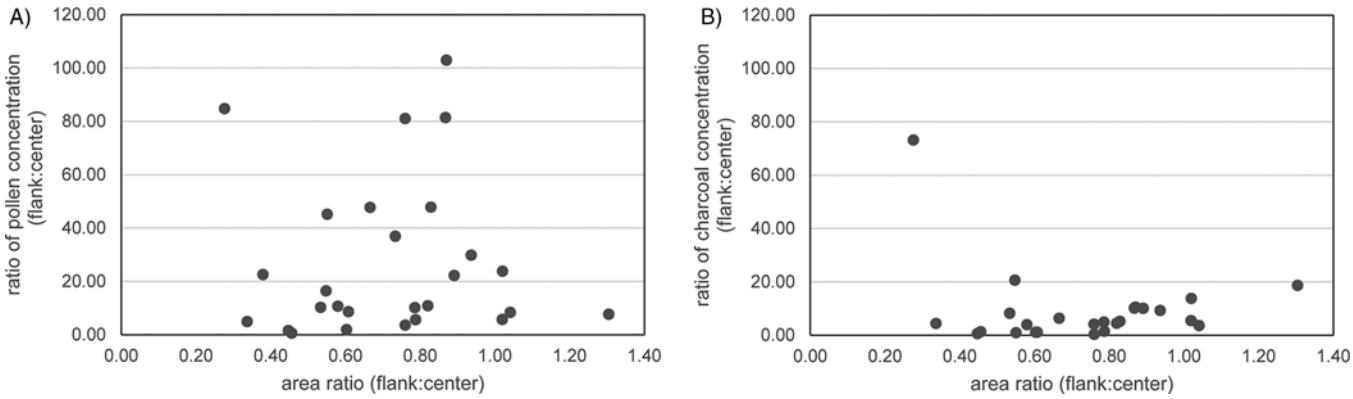

Figure 8. Comparisons of pollen and charcoal concentrations to the area ratio of samples. (**A**) Pollen concentrations, (**B**) charcoal concentrations.

indicates that there is no bias introduced by increased area to the pollen concentration or charcoal concentration of the stalagmites in this study.

DISCUSSION

The heterogeneity of pollen and charcoal concentrations within four stalagmites has been assessed by investigating whether pollen concentrations varied along isochronous horizons. It is clear that there is a large difference between central axis and flanks and spatial differences in concentration. Here we discuss whether those differences can be explained by differential transport of pollen on the stalagmite surface, or differential preservation of pollen on the stalagmite surface.

Controls on pollen and charcoal distributions

Previous studies into cave pollen assemblages suggest there are three potential modes of transport for pollen and charcoal into caves and onto speleothem surfaces: wind, water, and animal/insect vectors (Coles et al., 1989; Burney and Burney, 1993). Burney and Burney (1993) suggested that pollen is primarily transported into caves by wind. This theory was also demonstrated in a recent Australian palynological survey in the Nullarbor plain of Western Australia, where pollen grains were observed only on speleothems that also contained other evidence of wind-transported debris (Sniderman et al., 2016). The relationship between Th and pollen concentration seen in MC1 and 6J-2-13 corroborates this conclusion, because Th concentration is typically very low in 'clean' speleothem calcite, while high concentrations are usually associated with wind-blown clays (dust) or floodwaters bringing detrital sediments into the cave (Richards and Dorale, 2003). The correlation between Th concentration and pollen concentration is weaker in the Drovers Cave sample, a difference that may be influenced by differences in ventilation between the two caves. Mammoth Cave has two entrances as opposed to Drovers Cave which has only one. This would allow for a greater amount of wind-transported dust to move through Mammoth Cave and may explain the stronger relationship observed in MC-1. These results remain ambiguous because of the small sample size, but can be considered indicative, with promising potential for further exploration.

The higher concentrations of both pollen and charcoal on the flanks of the stalagmites examined in this study, as opposed to the central growth axis, suggest that air and water transport are the primary mode of both pollen and charcoal deposition (Fig. 9). Furthermore, each stalagmite has one side flank with a greater concentration of pollen and charcoal than the other (Figs. 2, 4), suggesting that the 'upwind' flank receives more airborne pollen, charcoal, and other detrital material than the opposite flank.

Transport bias, not preservation bias

Previous paleoecological studies have separately analyzed the resistance of pollen grains and charcoal fragments to degradation in various environments (Bryant and Holloway, 1983; Ascough et al., 2010; Scott, 2010). In general, pollen grains are more susceptible to degradation than charcoal in depositional settings that are important for paleo-studies (i.e., lakes, swamps, lacustrine environments). Notably, differences in degradation among subsamples were not observed here. However, when the concentration of both charcoal and pollen grains on the side flanks is compared to their respective concentrations on the central growth axis of their stalagmites, in every case the concentrations of both proxies were greater on the flanks of the stalagmite than then central growth axis. However, this does not imply that preservation is consistent throughout the stalagmites included in this study. The ratios of the pollen grain concentrations on the isochronous flanks and central axis are larger than the ratios of charcoal concentrations on the sides and center of the same stalagmites. This suggests either that pollen and charcoal particles do not behave the same way during transfer, or that the pattern of pollen found could result from the varying rate of degradation within the stalagmite and not a difference in distribution (Table 2). No distinguishable relationship is seen between the individual records beyond the general comment that samples with a larger charcoal concentration also typically contained a larger pollen concentration (Fig. 8). This implies there is either a relative loss of pollen at the central axis, or a relative gain of pollen at the flanks, compared to charcoal.

If greater concentrations of charcoal and pollen on the flanks of the stalagmites in Mammoth and Drover's Cave result solely from differences in preservation conditions along these gradients, observed concentrations of charcoal would not be expected to follow the same pattern because charcoal is oxidation resistant. Since both pollen and charcoal concentrations increase on the flanks, we propose that this pattern is generated primarily by transport of the detrital materials along the surface of the stalagmites. A plausible transport process may involve the pollen grains and charcoal fragments initially being transported into the cave

https://doi.org/10.1017/qua.2023.11 Published online by Cambridge University Press

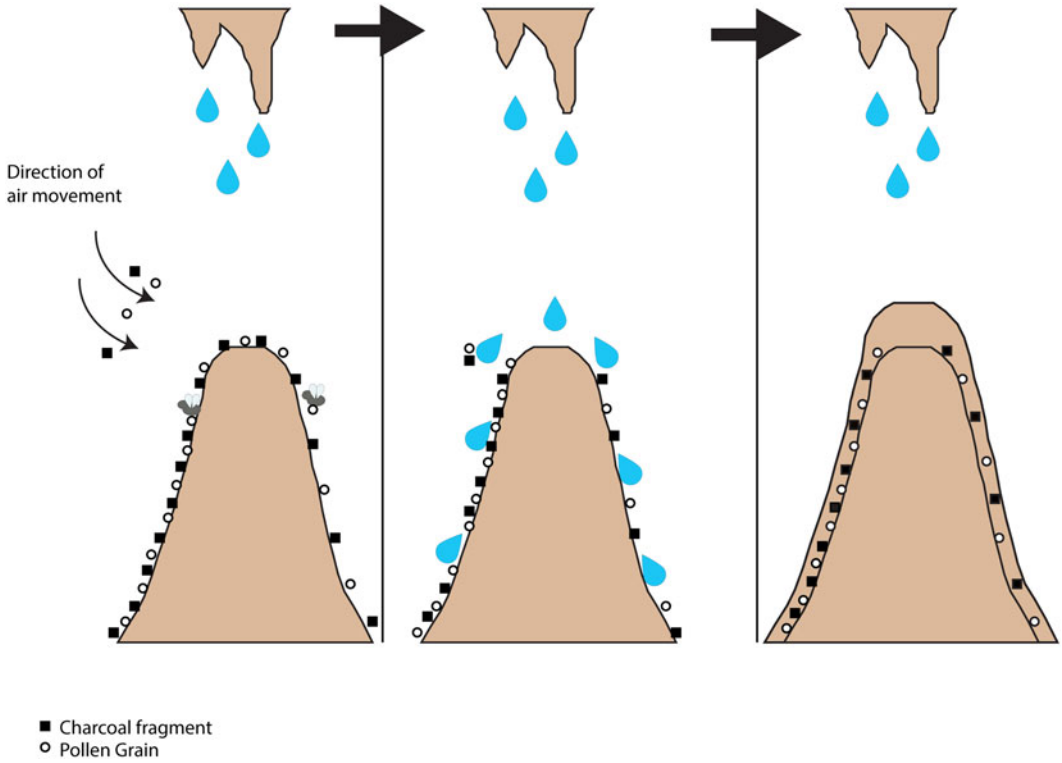

Figure 9. A schematic illustration of wind and water transport of pollen grains and charcoal fragments deposited by wind and animal vectors, then displaced by water droplets in Mammoth and Drovers caves.

chamber, presumably via air movement and insect vectors. The flank of the stalagmite that is oriented towards the cave entrance conceivably may collect a greater amount of pollen and charcoal on its surface. Drip water from the ceiling of the cave chamber strikes the stalagmite and moves a portion of charcoal fragments and pollen grains farther down the sides of the stalagmite, reducing the number of particles retained near the central growth axis. Some charcoal fragments and pollen grains also may be secondarily removed or relocated due to the force of the impact of the drip splash. The pollen grains and charcoal fragments become more concentrated on the flanks of the stalagmites because of these transport processes (Fig. 9).

Flank importance

Most speleothem studies have focused on stable isotopes of oxygen and carbon. In these studies, the flanks of stalagmites are avoided, because kinetic fractionation may influence the isotopic composition along the flanks (Hendy, 1971). However, as this study has demonstrated, in the field of speleothem palynology, the flank material of speleothems may be important to include when reconstructing fossil pollen assemblages. As illustrated in the pollen concentration heat maps along the growth axis of the stalagmites (Fig. 3), not only were the pollen and charcoal concentrations systematically enriched on the flanks relative to the central axis, but it is also evident that within every stalagmite there was one side flank that contained a greater concentration of pollen and charcoal. Neglecting to include this flank material would make fossil pollen analysis difficult, if not impossible, due to the low pollen concentrations at the central axis. This may go some way to explaining the very low concentrations of pollen encountered in some speleothems, where axial samples may have been used in order to compare with more traditional proxies (Festi et al., 2016; Honiat et al., 2022).

Another question that might arise is if this varying pollen concentration along a stalagmite might simply result from different volumes of the samples taken along the center axis and the flank. Despite pollen and charcoal concentration calculations accounting for a samples' mass, if a relationship between the pollen concentration of a sample and its surface area is evident, then there may have been some form of dilution of the samples in the fastest-growing, central part of each stalagmite. Given the consistent thickness of the stalagmite slice studied, the surface area of a sample can be used in lieu of its volume for this investigation. Here we demonstrated that there is no relationship between the ratios of the isochronous flank and center volumes of the samples and the ratio of pollen or charcoal concentrations (Fig. 8). This suggests that the distribution of pollen concentrations is not due to dilution introduced by the differing volume of the samples. Instead, we propose that a higher concentration of pollen grains and charcoal on one flank likely results from air movement within the cave chamber (Fig. 9).We hypothesize that the flank with the greater concentration of pollen and charcoal was likely facing the cave entrance (although this hypothesis clearly requires testing on stalagmites collected in growth position with known orientation, which were not available to us).

CONCLUSIONS

Using stalagmites from southwest Australia, this study provides new insights into the processes that transport pollen and charcoal into caves to be preserved on speleothem surfaces. The study outlines methods to improve our understanding of speleothem palynology and taphonomy and is the first to demonstrate that pollen

https://doi.org/10.1017/qua.2023.11 Published online by Cambridge University Press

grains and charcoal fragments are preferentially located on the side flanks of stalagmites compared to the central axis. We conclude that the distribution of pollen grains and charcoal within speleothems is influenced by transport of detrital particles along speleothem surfaces following deposition.

Acknowledgments. Speleothem samples used in this study were collected under permits from the Western Australian Government Department of Biodiversity, Conservation and Attractions, and with permission from the Margaret River Busselton Tourist Association. For assistance with permits and guidance in the field we thank David Henke and Mark Delane. Alan Grieg is thanked for assistance in the laboratory. This research was conducted with funding from the Australian Research Council under grant FL160100028 to JW.

Supplementary Material. The supplementary material for this article can be found at https://doi.org/10.1017/qua.2023.11

REFERENCES

APSA Members, 2007. The Australasian Pollen and Spore Atlas V1.0. Australian National University, *Canberra*. Available at: http://apsa.anu.edu.au/.

Ascough, P.L., Bird, M.I., Scott, A.C., Collinson, M.E., Cohen-Ofri, I., Snape, C.E., Le Manquais, K., 2010. Charcoal reflectance measurements: implications for structural characterization and assessment of diagenetic alteration. *Journal of Archaeological Science* **37**, 1590–1599.

Bryant, V.M., Jr., Holloway, R.G., 1983. The role of palynology in archaeology. In: Schiffer, M.B. (Ed.), *Advances in Archaeological Method and Theory*. Academic Press, USA, pp. 191–224.

Burney, D.A., Burney, L.P., 1993. Modern pollen deposition in cave sites: experimental results from New York State. *New Phytologist* **124**, 523–535.

Coles, G., Gilbertson, D., Hunt, C., Jenkinson, R., 1989. Taphonomy and the palynology of cave deposits. *Cave Science* **16**, 83–89.

de Porras, M.E., Mancini, M.V., Prieto, A.R., 2011. Modern pollen analysis in caves at the Patagonian steppe, Argentina. *Review of Palaeobotany and Palynology* **166**, 335–343.

Festi, D., Hoffmann, D.L., Luetscher, M., 2016. Pollen from accurately dated speleothems supports alpine glacier low-stands during the Early Holocene. *Quaternary Research* **86**, 45–53.

Hendy, C.H., 1971. The isotopic geochemistry of speleothems—I. The calculation of the effects of different modes of formation on the isotopic composition of speleothems and their applicability as palaeoclimatic indicators. *Geochimica et Cosmochimica Acta* **35**, 801–824.

Honiat, C., Festi, D., Wilcox, P.S., Edwards, R.L., Cheng, H., Spötl, C., 2022. Early last interglacial environmental changes recorded by speleothems from Katerloch (south-east Austria). *Journal of Quaternary Science* **37**, 664–676.

Leutscher, M., Moseley, G.E., Festi, D., Hof, F., Edwards, R.L., Spötl, C., 2021. A last interglacial speleothem record from the Sieben Hengste cave system (Switzerland): implications for alpine paleovegetation. *Quaternary Science Reviews* **262**, 10674. https://doi.org/10.1016/j.quascirev.2021.106974.

Matley, K.A., Sniderman, J.M.K., Drinnan, A.N., Hellstrom, J.C., 2020. Late-Holocene environmental change on the Nullarbor Plain, southwest Australia, based on speleothem pollen records. *The Holocene* **30**, 672–681.

McGarry, S.F., Caseldine, C., 2004. Speleothem palynology: an undervalued tool in Quaternary studies. *Quaternary Science Reviews* **23**, 2389–2404.

Meyer, M., Cliff, R., Spötl, C., Knipping, M., Mangini, A., 2009. Speleothems from the earliest Quaternary: snapshots of paleoclimate and landscape evolution at the northern rim of the Alps. *Quaternary Science Reviews* **28**, 1374–1391.

Nakagawa, T., 2013, *PolyCounter version 3.1.6*. http://polsystems.rits-palaeo.com/.

Playford, P.E., Cockbain, A.E., Low, G.H., 1976. Geology of the Perth Basin Western Australia. *Geological Survey of Western Australia, Bulletin* **124**, 1–311.

Richards, D.A., Dorale, J.A., 2003. Uranium-series chronology and environmental applications of speleothems. *Reviews in Mineralogy and Geochemistry* **52**, 407–460.

Scott, A.C., 2010. Charcoal recognition, taphonomy and uses in palaeoenvironmental analysis. *Palaeogeography, Palaeoclimatology, Palaeoecology* **291**, 11–39.

Sniderman, J.M.K., Hellstrom, J., Woodhead, J., Drysdale, R., Bajo, P., Archer, M., Hatcher, L., 2019. Vegetation and climate change in southwestern Australia during the last glacial maximum. *Geophysical Research Letters* **46**, 1709–1720.

Sniderman, J.M.K., Woodhead, J.D., Hellstrom, J., Jordan, G.J., Drysdale, R.N., Tyler, J.J., Porch, N., 2016. Pliocene reversal of late Neogene aridification. *Proceedings of the National Academy of Sciences* **113**, 1999–2004.

Woodhead, J.D., Hellstrom, J., Hergt, J.M., Greig, A., Maas, R., 2007. Isotopic and elemental imaging of geological materials by laser ablation inductively coupled plasma-mass spectrometry. *Geostandards and Geoanalytical Research* **31**, 331–343.

Woodhead, J., Sniderman, K., Hellstrom, J., Weij, R., MacGregor, C., Dickson, B., Drysdale, R.N., Delane, M., Henke, D., Bastian, L., Baynes, A., 2022. Timescales of speleogenesis in an evolving syngenetic karst: the Tamala Limestone, Western Australia. *Geomorphology* **399**, 108079. https://doi.org/10.1016/j.geomorph.2021.108079.